The Astrophysical Journal, 785:160 (12pp), 2014 April 20 doi:10.1088/0004-637X/785/2/160

THE GROUND-LEVEL ENHANCEMENT OF 2012 MAY 17: DERIVATION OF SOLAR PROTON EVENT PROPERTIES THROUGH THE APPLICATION OF THE NMBANGLE PPOLA MODEL

Christina Plainaki[1,2], Helen Mavromichalaki[2], Monica Laurenza[1], Maria Gerontidou[2], Anastasios Kanellakopoulos[2], and Marisa Storini[1]
[1] INAF-IAPS, Via del Fosso del Cavaliere, I-00133, Rome, Italy; christina.plainaki@iaps.inaf.it
[2] Nuclear and Particle Physics Section, Physics Department, National and Kapodistrian University of Athens, Pan/polis Zografos, 15771 Athens, Greece
Received 2013 November 6; accepted 2014 March 1; published 2014 April 7

ABSTRACT

In this work, we apply an updated version of the Neutron Monitor (NM) Based Anisotropic GLE Pure Power Law (NMBANGLE PPOLA) model, in order to derive the characteristics of the ground-level enhancement (GLE) on 2012 May 17 (GLE71), the spectral properties of the related solar energetic particle (SEP) event, the spatial distributions of the high-energy solar cosmic ray fluxes at the top of the atmosphere, and the time evolution of the location of the GLE source. Our modeling, based uniquely on the use of ground-level NM data, leads to the following main results. The SEP spectrum related to GLE71 was rather soft during the whole duration of the event, manifesting some weak acceleration episodes only during the initial phase (at ∼01:55–02:00 UT) and at ∼02:30–02:35 UT and ∼02:55–03:00 UT. The spectral index of the modeled SEP spectrum supports the coronal mass ejection–shock driven particle acceleration scenario, in agreement with past results based on the analysis of satellite measurements. During the initial phase of GLE71, the solar proton source at the top of the atmosphere was located above the northern hemisphere, implying that the asymptotic directions of viewing of the northern hemisphere NMs were more favorably located for registering the event than the southern ones. The spatial distribution of the solar proton fluxes at the top of the atmosphere during the main phase manifested a large variation along longitude and latitude. At the rigidity of 1 GV, the maximum primary solar proton flux resulted on the order of $\sim 3 \times 10^4$ part. m^{-2} s^{-1} sr^{-1} GV^{-1}.

Key words: acceleration of particles – solar-terrestrial relations – Sun: coronal mass ejections (CMEs) – Sun: flares

Online-only material: color figures

1. INTRODUCTION

Ground-level enhancements (GLEs) are short-term increases of the cosmic ray intensity registered at the ground by particle detectors, such as ionization chambers, muon, and neutron monitors (NMs), related to the arrival in the terrestrial environment of solar relativistic particles. Hence, GLE events are related to the most energetic class of solar energetic particle (SEP) events, associated with both solar flares and coronal mass ejections (CMEs), and requiring acceleration processes that produce particles with energies $\gtrsim$500 MeV upon entry in the Earth's atmosphere. In fact, this class of SEPs can produce showers of secondary particles with sufficient energy to be detected by ground-level NMs and with intensities that exceed the Galactic cosmic ray (GCR) background (see among others Lopate 2006; Reames 1999). During a GLE, the accelerated solar particles are mainly protons and, to a smaller extent, heavier ions, although some cases of GLEs associated with solar neutron emission have been also reported in the past (e.g., for GLE60; see Muraki et al. 2008). The intensities of SEP events resulting in GLEs are generally larger than those during normal gradual SEP events (e.g., Damiani et al. 2009; Mewaldt et al. 2012).

During the last seven solar cycles, 71 GLE events have occurred. On 2012 May 17, the first GLE of the 24th solar activity cycle, known as GLE71, was registered by the NMs of the worldwide network, starting at ∼01:51 UT (at Oulu) and having a maximum of about 17% (registered at the South Pole NM at ∼02:13 UT). Some examples of the GLE intensity time profiles registered at polar and mid-latitude NMs are presented in Figure 1. GLE71 occurred after a pause of about 5 yr from the previous GLE registered on 2006 December 13, i.e., several months after the predicted date from the forecast model by Pérez-Peraza (2011). Analysis of the satellite and the ground-level data showed that GLE71 was not a very large event, neither in intensity (The IceCube Collaboration 2013; Balabin et al. 2013; Kudela 2013) nor in energy of the arriving solar protons (Li et al. 2013).

Recent studies of GLE71 and of the respective SEP event, based either on the analysis and/or modeling of in situ and ground-based data, have shown that the event of 2012 May 17 is of particular interest. The most intriguing question related to GLE71 regards the determination of the acceleration mechanism that is responsible for the production of relativistic SEPs. In general, there are two main candidates: (1) acceleration at the flare reconnection sites, and (2) acceleration at the shocks driven by CMEs propagating through the solar corona and in the interplanetary space. Some recent analyses of the event of 2012 May 17 have shown that shock particle acceleration seems to be the most probable mechanism leading to the observed GLE (Firoz et al. 2012; Gopalswamy et al. 2013); however, a globally accepted acceleration scenario, consistent with the various multi-disciplinary analyses, does not exist (for high-energy impulsive GLEs, see the work performed by McCracken et al. 2012). Shen et al. (2013), based on an analysis of in situ data, argued that a "twin CME" scenario, as proposed by Li et al. (2013), could apply: two CMEs occurring in time much closer than any other pair in other GLE events (i.e., $\lesssim$3 minutes) could accelerate the particles that bounce back between the two shocks. According to these authors, the "twin CME" scenario could contribute to the whole accelerated particle population, which is efficiently produced mainly at the second shock according to Li et al. (2013). We note that Shen

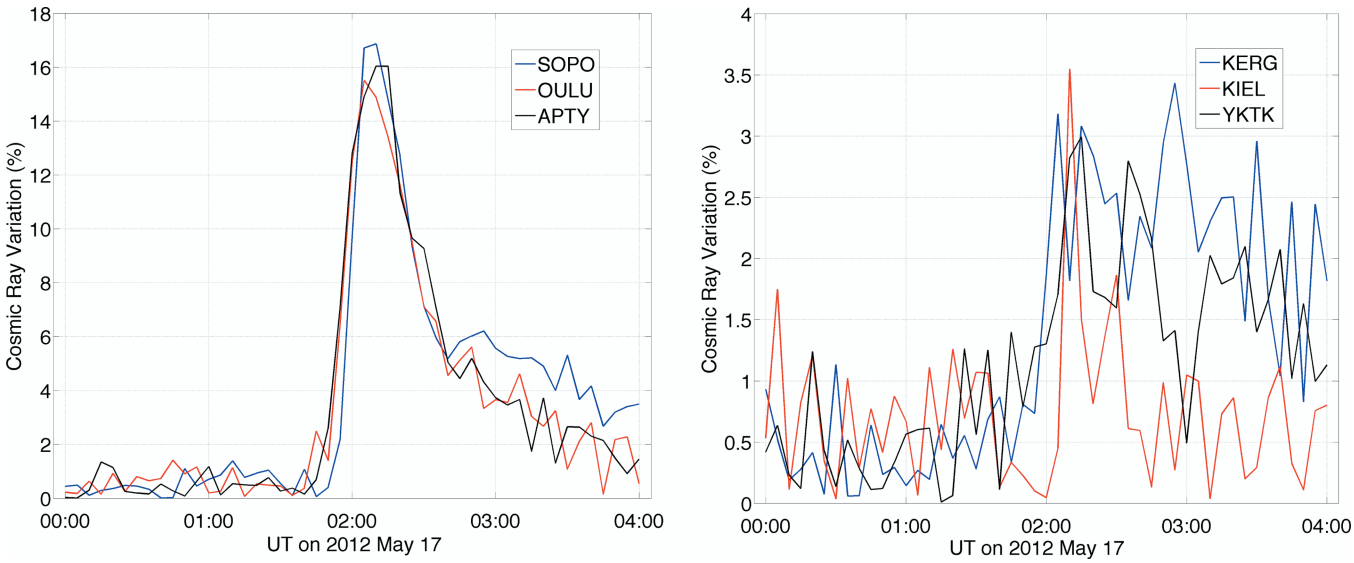

Figure 1. GLE of 2012 May 17 as observed by polar NMs (left panel) and mid-latitude NMs (right panel)—APTY: Apatity; OULU: Oulu; SOPO: South Pole; KERG: Kerguelen; KIEL: Kiel; YKTK: Yakutsk.

(A color version of this figure is available in the online journal.)

et al. (2013) also used particle data obtained at 1 AU from the Sun in their analysis; although these data provide direct information on the arriving SEPs (in this paper, also named as primary solar cosmic rays, SCRs), they regard a limited energy range for the solar particles, and therefore, information on the most energetic SEPs is not obtained. On the other hand, Li et al. (2013), on the basis of a multi-instrument data analysis and modeling, obtained evidence that GLE protons, with an estimated kinetic energy of ∼1.12 GeV, were probably accelerated by the CME-driven shock when it traveled to ∼3.07 solar radii.

One other important open issue on the GLE71/SEP event is the determination of the primary SCR spatial distribution at the top of the atmosphere. This information, however difficult to determine, is quite important since it is related to the characteristics of the solar particle injection at the Sun as well as to the conditions of the interplanetary space (i.e., interplanetary magnetic field (IMF), CMEs, solar wind) during the solar particle propagation. Balabin et al. (2013) determined the solar particle arrival direction during GLE71 for several different moments of the event. These authors found that at pitch angles close to 90° (the pitch angle is defined as the angle between the particle velocity direction and the IMF), an intensity gap in the primary SCR intensities is present during the GLE growth phase. This gap was due to the extremely low and quiet IMF under which GLE71 occurred, which resulted in an almost SEP scatter-free propagation in the interplanetary space along the magnetic field lines. According to Balabin et al. (2013), particles with large pitch angles would have significantly less drift velocity along the field line reaching the Earth than the particles propagating along the field, thus creating the observed gap.

One method to determine the direction of arrival of the solar particles at the Earth during a GLE is to model the ground-based NM data. Models can assume either a pitch angle distribution function (see Balabin et al. 2013 or Bütikofer et al. 2009) or, simply, a latitude and longitude-dependent function (that represents the spatial diffusion of the solar particles around the specific location of the source), without taking into consideration the IMF direction in modeling (see Plainaki et al. 2007, 2009a, 2010; Belov et al. 2005a, 2005b). Nevertheless, the determination of this parameter, through any of the techniques mentioned above, is not always unambiguous. For example, the alignment of the solar particle velocity with the IMF could be an indication of propagation along the magnetic field lines almost without scattering (Balabin et al. 2013). On the other hand, Bieber et al. (2002) argued that there is no reason that the magnetic field measured by a satellite at some point should be the same as the average field sampled by the particle over its orbit, given that the Larmor radius is of the order of the coherence length of interplanetary magnetic turbulence (Bieber et al. 2002; Bombardieri et al. 2007). For example, in the work of Bieber et al. (2002) on GLE59 (on 2000 July 14), the derived latitude of the anisotropy in the Geocentric Solar Ecliptic (GSE) coordinate system deviated from the IMF latitude up to almost 100° (opposite hemisphere) during the event maximum. Therefore, the apparent source vectors derived from the model do not need to be aligned with the measured magnetic field vectors; inversely, the model-assumption of particle propagation around the IMF vector is not always a quantity to be inserted a priori as an input.

Although some important efforts for deriving the properties of GLE71 (Balabin et al. 2013; Grigoryev et al. 2013) and the related SEP event (Li et al. 2013; Mewaldt et al. 2012; Shen et al. 2013; Gopalswamy et al. 2013) have been already performed, a complete interpretation of the GLE71 event features and a detailed determination of several important parameters are both still missing. An attempt to investigate GLE71 has been made by Bazilevskaya et al. (2013) who analyzed the GLE71 on the basis of the Payload for Antimatter Matter Exploration and Light-nuclei Astrophysics (PAMELA) instrument data (extending the direct measurements of the SEP energy range up to GeVs and covering the hundreds in the MeV region). These authors found good agreement with the ground-based installations (IceTop Air Shower Array and the NM world-wide network), except for the anisotropy phase of the GLE. Moreover, a joint discussion on the complete SCR spectrum from ∼10 MeV up to some GeVs, consisting of the lower energy part (obtained through fitting of theoretical functions to the observed satellite data; see Li

et al. 2013) and the relativistic part (obtained through NM data modeling; see, for example, Plainaki et al. 2010; Bombardieri et al. 2007), is missing. Such a connection between low-energy SCR and relativistic SCR could provide important information on the solar particle acceleration mechanism, the determination of which has been the subject of numerous debates (Cane et al. 2010; Lee et al. 2013). We underline that, in general, it is very difficult to model the SCR acceleration processes (Miroshnichenko & Pérez-Peraza 2008; Oreshina & Somov 2011) and to construct models and methods for predicting radiation hazard (Miroshnichenko 2003), since the primary SCR intensities are not always correlated with the actual energy range of the solar particles; for example, a considerable flux of relativistic particles does not mean that a powerful flux of protons will also be observed in the nonrelativistic region (Miroshnichenko et al. 2013). In this view, any information obtained through different theoretical, experimental, or observational methods (e.g., McCracken et al. 2012), including extrapolation of the modeled parameters in the lower rigidity range, can contribute to the existing knowledge and give some hints for the determination of the active SCR acceleration mechanism. Moreover, the independent modeling of the ground-based NM data during a GLE can provide spectral information on the event at an energy range where satellite data are either nonexistent or sparse.

In the current paper, GLE71 is studied through the application of the Neutron Monitor Based Anisotropic GLE Pure Power Law model (NMBANGLE PPOLA; Plainaki et al. 2010) using NM data of the European Neutron Monitor Database Network (NMDB, http://www.nmdb.eu). The scopes of the current paper are summarized in the following points.

1. To reconstruct the SCR spectrum in the relativistic energy range ($\gtrsim$500 MeV), at the top of the atmosphere.
2. To provide an estimation of the SCR spectrum in the lower energy range ($\lesssim$500 MeV), at the top of the atmosphere, through extrapolation of the model results.
3. To explain the form of the GLE time intensity profiles during GLE71 on the basis of the solar particle arrival directions and the NM asymptotic directions of viewing and their variation with time.
4. To provide quantitative information on various GLE characteristics, such as the main direction of the anisotropic flux arrival and the SCR intensity at the top of the atmosphere.

We underline that our study is based exclusively on the use of ground-based NM data; this technique is completely independent from the in situ measurements analysis, and therefore, an a posteriori comparison of specific model-derived quantities (e.g., the SCR spectrum) with the in situ measurements can be used to validate the model. In Section 2, we give a brief description of the solar, interplanetary, and near-Earth conditions during the event period and discuss the SEP/GLE71 observations. In Section 3, we give a brief description of the NMBANGLE PPOLA model, and in Section 4, we provide and discuss the results of the model application to GLE71. In Section 5, we draw the main conclusions of this work.

2. THE EVENT OF 2012 MAY 17

2.1. SEP Event-associated Observations

Early on 2012 May 17, the energetic particle sensor (EPS) of the *Geostationary Operational Environmental Satellites* (*GOES*) spacecraft recorded an increase in the proton and electron channels. The top panel of Figure 2 shows the flux profiles

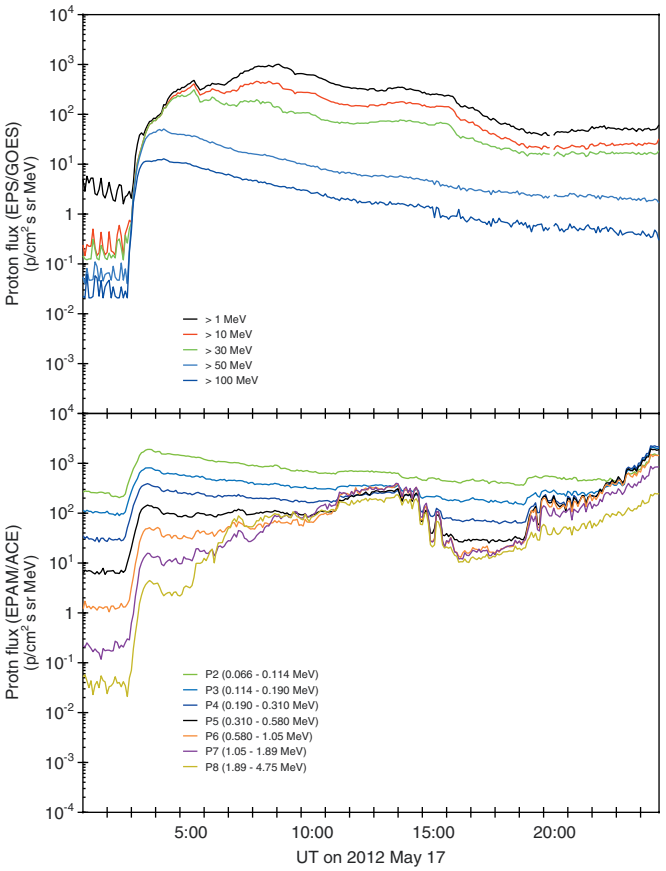

Figure 2. Temporal behavior of the proton integral (top) and differential (bottom) flux as recorded in different energy channels (energy reported in the legend) by EPS/*GOES* and EPAM/*ACE*, respectively, during the 2012 May 17 SEP event. The data were taken from http://www.ngdc.noaa.gov/stp/satellite/goes/dataaccess.html and http://www.srl.caltech.edu/ACE/ASC/level2/lvl2DATA_EPAM.html.

(A color version of this figure is available in the online journal.)

for protons of energies >10, >30, >50, and >100 MeV. The observed proton flux rise, at all of the energy channels, was fast and followed by a slower decay, which was still ongoing on 2012 May 18. Several minutes prior to these increases, a slow increase in the non-relativistic fluxes of electrons with energies >0.8, >2, and >4 MeV was also recorded. The 2012 May 17 SEP event extended to very high energies. Specifically, the >10 MeV proton event began at 02:10 UT, reached a peak flux of ~255 pfu at 04:30 UT, and ended at 16:20 UT on May 18. The >10 MeV flux crossed the ~100 pfu threshold at 02:45 UT, and it fell below ~100 pfu at 09:45 UT. Moreover, the >100 MeV proton event began at 02:00 UT, reached a maximum of ~20 pfu at 02:30 UT, and ended at 17:25 UT. At lower energies, the event was weaker than several SEP events that occurred in 2012 January and March. As shown in the bottom panel of Figure 2, the peak flux recorded by the Low Energy Magnetic Spectrometers instrument of the Electron, Proton and Alpha Monitor (EPAM) onboard the *Advanced Composition Explorer* (*ACE*) spacecraft was less than $\sim 10^3$ pfu in the differential energy channel 1.89–4.75 MeV/n. The PAMELA instrument, onboard the Russian satellite Resurs DK1, also recorded a significant flux of protons at energies lower than 1 GeV (Carbone et al. 2013), in reasonable consistency with the data of the *GOES* spacecraft and balloons in adjacent and overlapping energy

intervals, except for the *GOES* channel of 0.433 GeV which was always too high (Bazilevskaya et al. 2013).

The SEP event is associated with the M5/1*f* flare (peak time on May 17 at 01:47 UT) occurring in the active region (AR) 11476, located at N11W76. Based on the flare longitude, the SEP event was relatively "well-connected" to the source region, considering the observed solar wind speed of $\sim$400 km s^{-1} preceding the event. The event was accompanied by Type II (645 km s^{-1}) and Type IV radio sweeps, indicating the presence of a propagating interplanetary shock and a partial halo CME.

The CME was first observed by the Large Angle and Spectrometric Coronagraph C3 onboard the *Solar Heliospheric Observatory* (*SOHO*) spacecraft beginning at 02:06 UT, with an estimated plane-of-sky speed of $\sim$1200 km s^{-1}. The near-limb eruption was also observed by the coronographs and the EUVI instrument onboard the *Solar Terrestrial Relations Observatory* (*STEREO*) spacecraft. On 2012 May 17, *STEREO-A* was ahead of the Earth by 115°, so the eruption was at E39° in *STEREO-A* view. *STEREO-B* was 118° behind the Earth, so the CME was back-sided in *STEREO-B* view (source region at W194°; Gopalswamy et al. 2013). Shen et al. (2013) suggested that there were actually two eruptions (both from AR 11476) resulting in two CMEs, both fast and close in time to each other ($\lesssim$3 minutes). The eruption of the first CME (speed of $\sim$1258 $\pm$ 352 km s^{-1}) occurred at 01:29:33 UT, whereas the lift-off time of the second CME (speed of $\sim$1539 $\pm$ 352 km s^{-1}) was estimated to have occurred between 01:31 and 01:32 UT (Shen et al. 2013). This would support the "twin CME scenario," implying that the first CME-driven shock generated a very turbulent downstream region and pre-accelerated particles, which were reprocessed by the second CME driven shock. Shen et al. (2013) interpreted, indeed, the Type I radio burst episode as an indication of a shock–CME interaction (for description of this mechanism see Gopalswamy et al. 2001), whereas the second Type II radio burst episode could be due to the interaction of the two shocks driven by the two distinct CMEs. We note, however, that although the observations clearly manifested the appearance of two CMEs, the approach of Shen et al. (2013), closely resembling occurring sympathetic eruptions (Liu et al. 2009), is just one of the possible interpretations of the observations. Indeed, Gopalswamy et al. (2013), using *STEREO-A* data for height–time measurements, found that the CME height at the time of the GLE particle release (estimated to be 01:40 UT) was directly measured from a *STEREO* image as 2.32 *Rs*, which agrees well with the estimation from CME kinematics. Gopalswamy et al. (2013) also obtained the CME speed and acceleration elaborating the height–time measurements. According to these authors, the CME peak speed was $\sim$1997 km s^{-1} (at 01:40 UT), and the peak acceleration was $\sim$1.77 km s^{-2} (at 02:00 UT).

The overall geomagnetic field activity from 2012 May 15 until May 20 ranged from quiet to active levels. In particular, quiet levels were observed on May 15, 17, and 19. On May 16, an extended period of the southward B_z component of the IMF caused an isolated active level during the time lag from May 16, 21:00 UT until May 16 24:00 UT. No magnetic storm took place during the 2012 May 17 SEP event. The k_p index of geomagnetic activity was equal to 3 in the time interval between May 17 01:40–03:00 UT and equal to 2 in the time interval, May 17 03:00–03:30 UT. On May 20, at 01:36 UT, the *ACE* satellite observed an interplanetary shock passage with a corresponding weak sudden impulse observed in the Boulder magnetometer ($\sim$15 nT) at the same day on 02:15 UT, likely associated with the CME on May 17. The geomagnetic field responded with an isolated active period during the time period from May 20 03:00 UT until May 20 06:00 UT.

2.2. Neutron Monitor Observations

Secondary particles, associated with the SEP event described in the previous paragraph, were detected by the ground-level NMs of the worldwide network on 2012 May 17. The intensity time profiles based on five minute data, registered at three polar NMs, are shown in Figure 1 (left panel). The pre-increase baseline period used to derive the GLE71 percentage was set at 2012 May 17 00:00–01:00 UT. The GLE was seen mostly by polar and some mid-latitude NMs. Specifically, on the basis of the five minute data, the polar NM of South Pole (SOPO) registered a maximum of about 17% at 02:05 UT, whereas the northern polar NMs of Oulu (OULU) and Apatity (APTY) registered maxima of about 16% (at 02:05 UT) and 15% (at 02:15 UT), respectively (Figure 1, left panel). Moreover, the Polar Bare neutron detectors (i.e., an array of 12 bare (without lead) neutron detectors) showed a clear pulse-like enhancement with a peak just after 02:00 UT (The IceCube Collaboration 2013) at SOPO. The count rates of these detectors have a larger percentage increase than the NM64 rates because they respond more to lower energy particles, and the solar spectrum is softer than the GCR spectrum (The IceCube Collaboration 2013). For this reason, the event of 2012 May 17 was registered by the Polar Bare detectors with a bigger percentage increase with respect to the signal registered by the standard NM64 at the South Pole.

Among the numerous mid-latitude NMs, GLE71 was registered at Kiel (KIEL), with a maximum increase of $\sim$3.6% (at 02:10 UT); at Kerguelen (KERG), which recorded two maxima, the first one equal to $\sim$3.2% (at 02:05 UT) and the second one equal to $\sim$3.4% (at 02:55 UT); and at Yakutsk (YKTK), which registered a maximum of $\sim$3% (at 02:15 UT) (Figure 1, right panel). According to the data selected from the NMDB, the GLE71 was registered by at least 17 NMs of the worldwide network. The low-latitude NMs (high magnetic cut-off rigidity, R_c) did not register GLE71 (e.g., Signoretti & Storini 2013). This observation, together with the fact that GLEs are mainly due to solar protons, implies that the maximum rigidity of the primary solar protons could not have been higher than $\sim$2.4 GV. A more detailed search for small time scale records of other detectors than those used in this study is intended for the near future but is beyond the scope of this paper. In general, a first-order analysis of the ground-based observations shows that the GLE71 turned out to be rather small in both intensity and primary solar proton energy.

3. MODELING

In this study, we derive the characteristics of the SEP event responsible for the GLE on 2012 May 17, through the application of the NMBANGLE PPOLA model (Plainaki et al. 2010). The NMBANGLE PPOLA model is a slightly modified version of the original NMBANGLE model (Plainaki et al. 2007), which is based on the coupling coefficient method (Dorman 2004) applied numerous times in the past (e.g., Belov et al. 2005a, 2005b; Plainaki et al. 2007, 2010). As inputs, the model uses the cosmic ray GLE data from NM stations widely distributed around the world. Our model treats the NM network as an integrated omnidirectional spectrometer able to measure the characteristics of the relativistic primary SCR flux at some point of the near-Earth magnetosphere. In this context, modeling

of the NM response to an anisotropic SCR flux and solving the inverse problem can provide the actual characteristics of the relativistic SEPs that are responsible for the event (Shea & Smart 1982; Humble et al. 1991; Cramp et al. 1997). The results of the application of both NMBANGLE and NMBANGLE PPOLA models to past GLEs have been, in general, in good agreement with the observations, when available (Plainaki et al. 2007, 2009a, 2010). The details of the physics that the NMBANGLE PPOLA model uses have been provided in the past (see Plainaki et al. 2007, 2010); moreover, a description of the modifications implemented in the NMBANGLE PPOLA model (with respect to the previous model version) has been provided analytically by Plainaki et al. (2010). For this reason, in this section we simply give a brief description of the model and of the necessary modifications in order to apply it to GLE71.

The NMBANGLE PPOLA model couples primary SCRs at the top of the Earth's atmosphere with the secondary ones detected at ground-level NMs during GLEs. This model dynamically calculates the SCR spectrum and the SCR flux spatial distribution outside the atmosphere, assuming a power-law spectrum for the primary SCRs. For the evaluation of the NM asymptotic directions of viewing, we applied the method described by Plainaki et al. (2009b) assuming that the Earth's magnetospheric field can be adequately described by the Tsyganenko (1989) model. Summarizing, the NMBANGLE PPOLA model uses, as inputs, the response of the worldwide neutron monitor network to the high-energy solar protons (i.e., $>\sim$500 MeV) and the disturbance level of the geomagnetic field (through the use of the k_p index). In its current version, the model assumes that the primary SCR particles during this event are only protons.

According to the NMBANGLE PPOLA model, the possible time variations, $\Delta N/N_0$, of the total neutron counting rate, N_0, observed at cut-off rigidity, R_c, at level h in the atmosphere at some moment t, are determined by the following expression (Dorman 2004; Belov et al. 2005a, 2005b; Plainaki et al. 2010):

$$\frac{\Delta N(R_c, h, t, t_0)}{N_0(R_c, h, t_0)} = \int_{R_c}^{R_u} \frac{W(R, h, t_0) \cdot A(R, \Omega(R, t), t) \cdot b(t) R^{\gamma(t)}}{I_0(R, t_0)} dR, \quad (1)$$

where $W(R, h, t_0)$ is the rigidity-dependent coupling function between secondary and primary cosmic rays arriving at the top of the atmosphere (see Plainaki et al. 2007 for analytical expression); $\gamma(t)$ is the exponent of the power-law primary SCR spectrum (i.e., at the top of the atmosphere); $A(R, \Omega, t)$ is a dimensionless normalized function that describes the spatially anisotropic arrival of the SCR at 1 AU, with $\Omega(R, t)$ being the solid angle defined by the vertical asymptotic directions of a NM at rigidity R and the location of the SCR source at the same altitude, as defined in Plainaki et al. (2007); R_u is the theoretical upper limit for the rigidity of the primary SCR particles; $b(t)$ is the amplitude of the primary SCR differential flux (in protons $m^{-2}\,s^{-1}\,sr^{-1}\,GV^{-1}$); and $I_0(R, t_0)$ is the GCR differential flux (in protons $m^{-2}\,s^{-1}\,sr^{-1}\,GV^{-1}$). In our model, we define $A(R, \Omega(R, t), t)$ as in Plainaki et al. (2007):

$$A(R, \Omega, t) = \exp\left(-n_a(t)^2 \sin^2 \frac{\Omega(R, t)}{2}\right), \quad (2)$$

where $n_a(t)$ is a dimensionless parameter that characterizes the width of a primary solar particle beam arriving at the top of the Earth's atmosphere, focused above some specific location. Through the selection of the mathematical form described in Equation (2), our model parameterizes the level of the primary SCR anisotropy by the use of variable n_a, which is dynamically determined after each model run. Big values for n_a mean that the main SCR arrival direction is focused around a specific location, whereas smaller values for n_a mean that the SCR flux is distributed more widely in longitudes and latitudes. This parameter is determined independently from the magnitude of the primary SCR intensity. All calculations using Equations (1) and (2) in the NMBANGLE PPOLA model refer to the top of the atmosphere.

The total output of the model application is a multidimensional (i.e., in space and energy) GLE picture that attempts to describe the solar particles' behavior under extreme solar conditions. In this analysis, the particle trajectories calculated in order to define the NM asymptotic directions are conisdered only for particles with vertical incidence. This restriction can imply limitations in case of highly anisotropic events (such as those in 1989 September and in 1956 February); in such cases, a nonvertical SCR arrival can produce an NM response that a vertical incidence would not (Cramp et al. 1995). This is also the case where the east–west asymmetry becomes important for the high cut-off monitor observations. However, low cut-off rigidities (below 5 GV) do not strongly depend on the direction of the particles' arrival (Dorman et al. 2008). Moreover, Bazilevskaya et al. (1996) have found that the low rigidity protons arriving from different zenith and azimuthal directions at a given time have very close asymptotic directions. Therefore, since the majority of the stations used for the analysis of this event are low and middle cut-off rigidity stations, we assume that the consideration of explicitly vertical incidence proton directions does not compromise the results. Moreover, in our particle trajectory calculation, we consider that the relativistic SEPs arrive to an altitude of $\sim$20 km above the sea level. The primary scope of the NMBANGLE PPOLA is to reproduce the observed SCR increases and to define the time evolution of several GLE parameters (i.e., spectral index, spatial distribution of the SCR flux outside the atmosphere, etc.). A least-squares fitting technique based on the Levenberg Marquardt algorithm allows an efficient derivation of the optimal solution for each time interval and the determination of the GLE parameters evolution.

Five-minute GLE data from 29 NM stations of the NMDB network (see Table 1), were incorporated to fit Equation (1). These data were modeled every five minutes between 01:40 UT and 03:30 UT. Each time represents the start of a five minute integrated time interval. For evaluation of the NM asymptotic directions of viewing, we applied the method described in Plainaki et al. (2009b).

4. RESULTS AND DISCUSSION

In order to validate the quality of our fit, we calculate the correlation coefficient, C, between the modeled and observed values of the NM intensity variations. This parameter is a measure of the strength of the linear relationship between these two quantities, and therefore, it characterizes the goodness of the actual fit. It should be kept in mind, however, that GLEs are technically difficult to model, in general. The main reason for this is the lack of a certain theory that adequately describes the SCR spectrum over the whole rigidity range where the response of the ground-level NMs to SEP events is possible. The actual calculation can become even more difficult in the following cases: (1) when the enhancements registered at the NMs are relatively small, for example, in the initial phases of

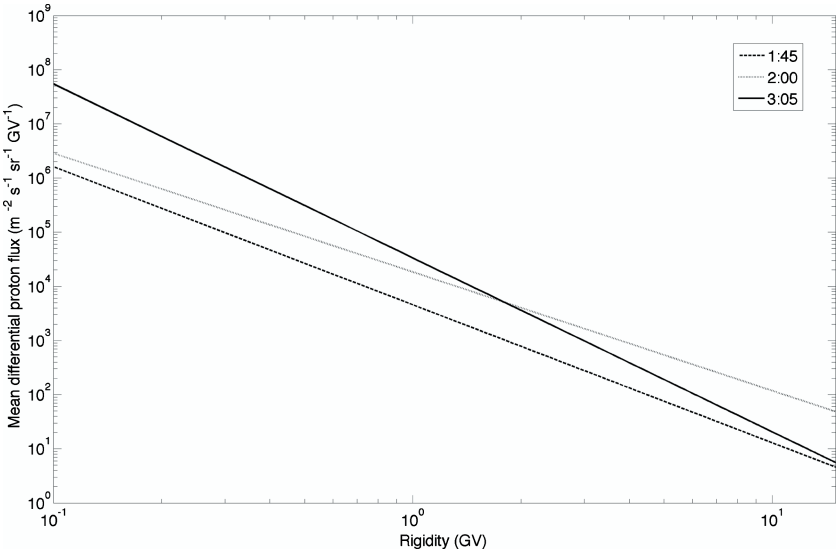

Figure 3. Primary solar proton rigidity spectrum at different moments of the event, at the top of the Earth's atmosphere, as derived by the NMBANGLE PPOLA model application.

Table 1
Characteristics of the NMs Used in This Analysis

Station	Latitude (deg)	Longitude (deg)	*Rc* (GV)	Altitude (m)
Almaty	43.14	76.60	6.69	3340
Apatity	67.57	33.40	0.65	181
Athens	37.58	23.47	8.53	260
Baksan	43.28	42.69	5.60	1700
Emilio Segrè Observatory	33.30	35.80	10.75	2055
Fort Smith	60.02	−111.93	0.30	180
Inuvik	68.36	−133.72	0.30	21
Irkutsk	52.47	104.03	3.64	Sea level
Irkutsk 2	52.47	104.03	3.64	2000
Irkutsk 3	52.47	104.03	3.64	3000
Jungfraujoch	46.55	7.98	4.50	3570
Jungfraujoch 1	46.55	7.98	4.50	3475
Kerguelen	−49.35	70.25	1.14	33
Kiel	54.34	10.12	2.36	54
Lomnický Štít	49.20	20.22	3.84	2634
McMurdo	−77.90	166.6	0.30	48
Magadan	60.04	151.05	2.09	220
Moscow	55.47	37.32	2.43	200
Nain	56.55	−61.68	0.30	46
Norilsk	69.26	88.05	0.63	Sea level
Newark	39.68	−75.75	2.40	50
Oulu	65.05	−25.47	∼0.80	15
Peawanuck	54.98	−85.44	0.30	53
Rome	41.86	12.47	6.27	Sea level
South Pole	−90.00	0.00	0.10	2820
Terre Adeliè	−66.65	140.00	∼0.00	32
Thule	76.50	−68.70	0.30	26
Tixie Bay	71.36	128.54	0.48	Sea level
Yakutsk	62.01	129.43	1.65	105

Note. Data derived from the NMDB Database, http://www.nmdb.eu

the event (see Section 3.1. in Plainaki et al. 2010) or during low intensity events (e.g., GLE71); and (2) when the NM data used in the analysis are not equivalently distributed in longitudes and latitudes (i.e., specific magnetic locations are covered more than others), and therefore, the fit algorithm is forced to derive a biased preferential direction for the arriving primaries. Indeed, a detailed investigation on the reasons of the existence of different results obtained through modeling of the same event is found in Bütikofer & Flückiger (2013). Recent studies have pointed out the particularity of the GLE of 2012 May 17 and, hence, the difficulty in modeling its behavior. After applying an advanced modeling technique, already tested in many GLEs of the past, Balabin et al. (2013) argued that a suitable solution could not be derived for a given form of the pitch-angle distribution for GLE71. These authors attributed this difficulty to the fact that at pitch angles close to 90°, an intensity gap is present; to overcome this problem they created a special function to add a gap into Gaussian distribution at ∼90° and obtained updated fitting solutions with a satisfactory accuracy (∼10%–15%).

The fit, performed using the NMBANGLE PPOLA model, was found to be mostly reliable in the time period from 01:55 UT until 02:45 UT, where the correlation coefficient, *C*, was in the range of 50%–93% (the best fit was obtained for the time lag 01:55–02:00 UT). In the next time intervals, the fit was generally satisfactory except for the time interval 02:45–02:50 UT, when the correlation coefficient was extremely low (∼40%, i.e., the lowest value in the whole fitting period). The standard deviation was small for all of the fitting time intervals (ranging from 0.4% to 4%). The parameter values, discussed in the next paragraphs, were obtained with a satisfactory accuracy ($\sim 2\sigma$).

4.1. Primary SCR Spectrum and Anisotropy

In Figure 3, we present the rigidity spectrum of the primary solar protons, as derived by the application of our model at different intervals: 01:45–01:50 UT (i.e., prior to the GLE onset), 02:00–02:05 UT (when all polar stations have already registered the GLE onset), and 03:05–03:10 UT (i.e., close to the time of the >100 MeV maximum flux). It is clearly seen, that during this GLE, the temporal variations in the primary SCR spectrum were small, suggesting a rather soft spectrum of accelerated protons. Indeed, according to the outputs of the NMBANGLE PPOLA model application, the rigidity spectral index varies between –3.8 and −2.1 (Figure 4, upper panel), with the hardest spectrum obtained in the time interval 01:55–02:10 UT. This result is in good agreement with the Li et al. (2013) findings, indicating, on the basis of satellite and NM observations, a rather soft solar particle

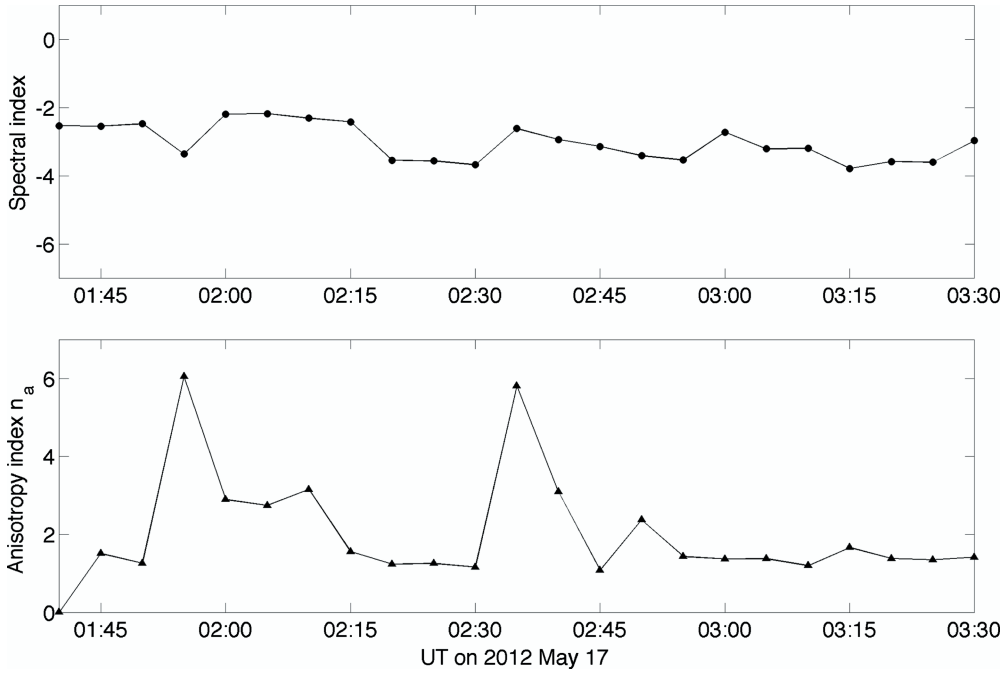

Figure 4. Time evolution of the spectral index of the primary solar protons (upper panel) and the anisotropy index (lower panel), at the top of the Earth's atmosphere, as derived by the application of the NMBANGLE PPOLA model.

energy spectrum during GLE71. It is worthwhile to note that the application of our model suggests the possible existence of two small secondary episodes of solar particle acceleration (indicated by a hardening of the solar proton spectrum) at the time intervals 02:30–02:35 UT and 02:55–03:00 UT. We note that the observed proton flux >100 MeV registered at *GOES* (Figure 2) was at a high level during the whole hour (02:00–03:00 UT) and had a small increase during the time interval 03:00–03:30 UT (see also Figure 9 reported by Li et al. 2013). Therefore, the existence of two acceleration episodes, as revealed by the ground-based data modeling, cannot be excluded. Of course, any indication for solar proton acceleration obtained by the results of the NMBANGLE PPOLA model application is rigorously valid only in the proton rigidity range that corresponds to the NM measurements, i.e., $\gtrsim$1 GV. Any information obtained by the model for the lower rigidity particles is the result of an extrapolation and should be treated with caution. Moreover, Adriani et al. (2011) recently showed that the SCR spectra obtained by NM data modeling in the energy range <700 MeV is always softer than the one obtained by the PAMELA space experiment (Picozza et al. 2007), probably due to underestimated NM yield functions in this energy range.

The spectral index of the differential rigidity spectrum obtained by the NMBANGLE PPOLA model application (see Figure 4, upper panel) for the main phase of the event (after 02:20 UT) is approximately −3.8. In order to evaluate whether the differential rigidity spectrum at lower rigidities, obtained through our model, is consistent with the analysis of the event of 2012 May 17 based on the existing observations of particle fluxes (e.g., Li et al. 2013), we firstly perform a rough transformation of our modeled parameters. Specifically, we transform the rigidity spectrum assumed in our model (i.e., $b\,R^{\gamma}$) to energy spectrum through the following equation, applicable for the nonrelativistic case:

$$b \cdot R^{\gamma} dR = c \cdot E_p^{\frac{\gamma-1}{2}} dE_p, \quad (3)$$

where E_p is the proton energy of a solar proton of rigidity R, and c is a constant. On the basis of Equation (3), we get that the power-law index of the energy spectrum is $\alpha = (\gamma - 1)/2$, with γ being the spectral index of the rigidity differential spectrum. So, on the basis of the NMBANGLE PPOLA model application, during the main phase of the event, α is about −2.4. This result can be considered to be consistent with the estimation by Li et al. (2013), who found that $\alpha = -3.2$. We underline that Li et al. (2013) arrived at this estimation using a different method, i.e., these authors used combined in situ particle observations and ground-level measurements in order to fit a power-law energy spectrum with an accuracy factor equal to about 2.0.

Note that, any estimation obtained by our model for the lower energy solar particles is expected to correspond to a softer spectrum than the one obtained through the satellite data. This happens because our method is based on the extrapolation of the power law obtained through the use of ground-level NM data (that correspond to the higher energy range of the SEPs), which tends to overestimate the flux at nonrelativistic energies (for instance, the exponential rollover and the streaming limit are not taken into account).

The hardest energy spectrum value obtained by the NMBANGLE PPOLA model, corresponding to the initial phase of the event being equal to −1.55, is within the typical range found by Ellison & Ramaty (1985) for shock wave acceleration in the case of nonrelativistic SEP events; indeed, according to the Ellison & Ramaty (1985) results, for weak to moderated strength shocks, magnetic field components parallel to the shock, and typical solar conditions, the spectral index of the differential energy spectrum should vary between −3.00 and −1.25. However, as noted by Berezhko & Taneev (2003) and Li et al. (2013), the approximation of Ellison & Ramaty (1985) is applicable to a bulk of accelerated particles in the vicinity of the shock and not to the range of ultimate energies; hence, it results in a significant softening of the particle spectrum and a decrease in their maximum energy. The extrapolated results obtained by our model do not contradict the scenario of a possible shock wave

acceleration during the event of 2012 May 17, also suggested by other studies (e.g., Li et al. 2013; Gopalswamy et al. 2013; Shen et al 2013). Although further analysis is necessary in order to achieve a more accurate determination of the acceleration mechanism, we suggest that the application of the NMBANGLE PPOLA model to the NM data on 2012 May 17 supports the shock wave acceleration scenario, without excluding other possible mechanisms (e.g., stochastic acceleration in turbulent plasma, connected to an expanding CME, as suggested by Vashenyuk et al. 2011).

Recently, an important effort to derive the solar particle energy spectrum for the initial phase of GLE71 was made by The IceCube collaboration (2013), who separately analyzed the counting rates of the multiple discriminator thresholds in IceTop (the surface component of the IceCube Neutrino Observatory) as well as the measurements registered by NM64 and the Polar Bare neutron detectors at the South Pole. These authors found that the spectrum derived from the IceTop analysis was not consistent with the one derived from the NMs/Polar Bare analysis over most of the NM response range (i.e., at rigidities >1 GV) with the latter being significantly less steep. Our results, based on the application of the NMBANGLE PPOLA model, are not consistent with the spectrum derived through the IceTop analysis, which is sensitive to higher energies than the NMs. A possible reconciliation is that the actual spectrum exhibits a major steepening at a significantly high energy where it cannot be adequately described by a power law. Nevertheless, The IceCube collaboration (2013) underlined that significant modifications in their air shower analysis are required in order to determine a complete and accurate set of yield functions for IceTop, since most of the information on solar events comes from signals with amplitudes below the one corresponding to the instrument threshold (Abbasi et al. 2013). On the other hand, the potential use of dynamically varying NM yield functions (pressure, air, and temperature dependent) while modeling NM data could have an impact on the derived spectrum. Therefore, we believe that further progress is required in order to shed light on this inconsistency between different types of ground-based data.

As previously discussed in Section 2, GLE71 appears to be anisotropic in its initial phase. In Figure 4 (lower panel), we present the time evolution of the model parameter, n_a characterizing the level of the primary SCR anisotropy. It is clearly seen that the most anisotropic particle arrival took place in the time intervals 01:55–02:00 UT ($n_a = 6$, 1) and 02:35–02:40 UT ($n_a = 5$, 8). Indeed, in the polar NM intensity time profiles (see Figure 1, left), it is clearly seen that the northern polar station registers significantly higher fluxes in the 01:55–02:00 UT interval; moreover, in the 02:35–02:40 UT interval, both northern polar NMs, APTY and OULU, register higher count rates than the southern NM SOPO. The differences are smoother in the intermediate phase.

The direction of the apparent source of solar particles, a quantity that is generally difficult to determine, is a dynamical output of the NMBANGLE PPOLA model. The time-dependent variation of the position of the most intense solar particle source near Earth, in geographical coordinates, is illustrated in Figure 5. In the initial phase, the apparent SCR source direction was located in the Northern hemisphere, whereas with time, it moved to lower latitudes. We find that the position of the apparent SCR source at the top of the atmosphere, as derived by our model, is not aligned with the IMF direction, which was relatively stable during GLE71 (Balabin et al. 2013).

Balabin et al. (2013) also claimed that GLE71 was anisotropic, and they modeled the event assuming a complex Gaussian-like (in pitch angle distribution) anisotropy form that differed from the one considered in the current study. These authors argued that the choice of the anisotropy form in their model was made in order to fit the intensity gap observed at the NM counting rates at pitch angles close to $\sim 90^\circ$. The accuracy of the fitting obtained by Balabin et al. (2013) may have been satisfactory; however, their assumption has a crucial difference with the one in the NMBANGLE PPOLA model. Balabin et al. (2013) assume a priori that during GLE71, the particles propagated along the magnetic field lines almost without scattering, whereas in the NMBANGLE PPOLA model, no such assumption is being made. On the contrary, our model determines the location of the arrival of the SCR anisotropic flux independently from the measured (by a satellite) IMF direction. Given that the Larmor radius is of the order of the coherence length of interplanetary magnetic turbulence (Bieber et al. 2002; Bombardieri et al. 2007), we believe that there is not reason to impose the condition that the magnetic field should be the same as the average field sampled by the particle over its orbit in modeling. Future investigations, including extended analyses of satellite measurements of plasma and the magnetic field at 1 AU from the Sun, could shed light on this direction.

4.2. Primary SCR Source and Fluxes

The average, over all space, of modeled SCR fluxes with energies >100 MeV, >500 MeV, and >1000 MeV, reaching the upper atmosphere on 2012 May 17, is presented in Figure 6. In the same plot, we also show the observed integral flux of protons with energies >100 MeV, as obtained by *GOES* 15 data. We underline that the NMBANGLE PPOLA model is based on the use of ground-level NM data, and therefore, any result is rigorously valid when referring to primary SCR energies $\gtrsim 500$ MeV. In fact, any extrapolation of the model results in the energy range $\lesssim 500$ MeV assumes that the lower energy solar particles behave in the same way as the higher energy particles. Nevertheless, in Figure 6, it is clearly seen that the fluxes obtained by our model are in good agreement with the observed fluxes in the time interval 02:05–03:35 UT, i.e., when the >100 MeV flux reaches its maximum value and all NMs have already registered the onset of the GLE. On the contrary, in the initial phase of the event, when the solar proton arrival is anisotropic, the spatially average modeled fluxes do not adequately represent the real situation. Figure 6 shows that the modeled fluxes in the time period 1:40–02:05 UT are significantly higher than the observed ones. The largest difference between modeled and observed values appears in the time interval 01:50–01:55 UT, i.e., when only a few northern NMs have registered the GLE onset. In the time interval 02:00–02:05 UT, the integral proton flux >100 MeV registered at *GOES* 15 was, on average, 0.4 pfu, which is ~ 10 times lower than the average value derived from the model. The disagreement of our modeled results with the observations in the initial phase of the GLE, as presented in Figure 6, is due to the nature of our model and specifically due to the averaging of an initially anisotropic SCR flux (see the NM time profiles in Figure 1, left) over all space. To demonstrate this more clearly, in Figure 7, we plot the latitude–longitude contour plots of the equal integral proton fluxes for particles with energies >100 MeV, at the top of the Earth's atmosphere, using the outputs of the NMBANGLE PPOLA model application. In the same plot, we also present the

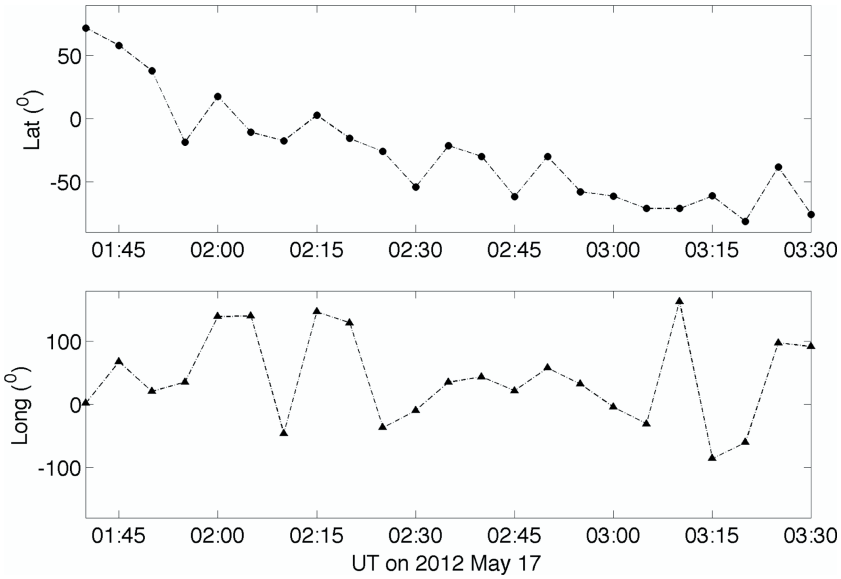

Figure 5. Time evolution of the position of the apparent SCR source, at the top of the Earth's atmosphere, as derived by the application of the NMBANGLE PPOLA model.

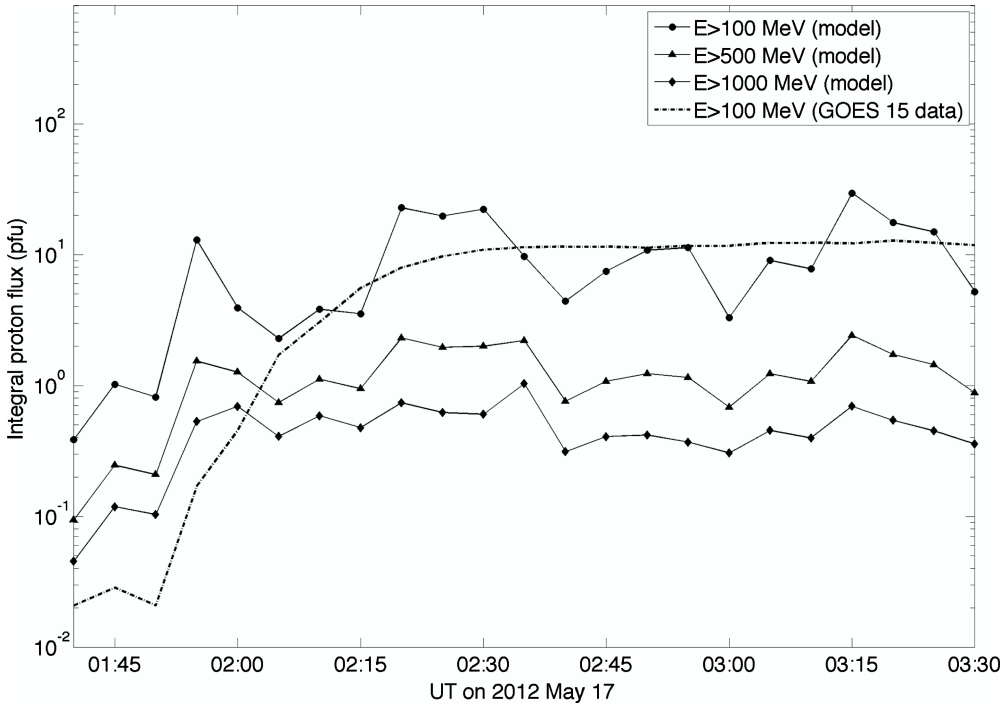

Figure 6. Average (over latitude and longitudes) integral solar proton fluxes at different energies, at the top of the Earth's atmosphere, as derived by the application of the NMBANGLE PPOLA model. The *GOES* proton flux of particles with energy >100 MeV is also plotted.

asymptotic directions of viewing for some NMs, calculated by application of the method described by Plainaki et al. (2009b). Figure 7 shows that the average integral proton flux (>100 MeV) of ∼4 pfu (1 pfu is equal to 1 part. cm^{-2} s^{-1} sr^{-1}), corresponding to the time interval 02:00–2:05 UT (presented in Figure 5), is in reality subject to local variations determined by the direction of the arrival of the particles. According to the model, the spatially varying primary SCR flux (>100 MeV) ranges between ∼0.8 pfu and ∼7 pfu. The lower limit of this range is only a factor of two higher than the observed value. Therefore, the disagreement between our modeled SCR fluxes and the observed ones is due to the technical treatment of the model output and not due to the inadequacy of the model in describing the real situation. However, the extrapolation of the results of our model in the lower energy range ignores the time delay in the arrival of these particles at 1 AU, which would result in a diminishing of the extrapolated fluxes. On the basis of the above considerations, we can deduce that our model can give some realistic information even in the energy range down to 100 MeV, since it reproduces the observations in a satisfactory way. Further modeling in the lower energy range, using satellite data, is intended in the future but is beyond the scope of this paper.

Using the outputs of the NMBANGLE PPOLA model application, we calculate the latitude–longitude contour plots of equal differential proton fluxes at the top of the Earth's atmosphere for two different time intervals of the event: 1:50–1:55 UT

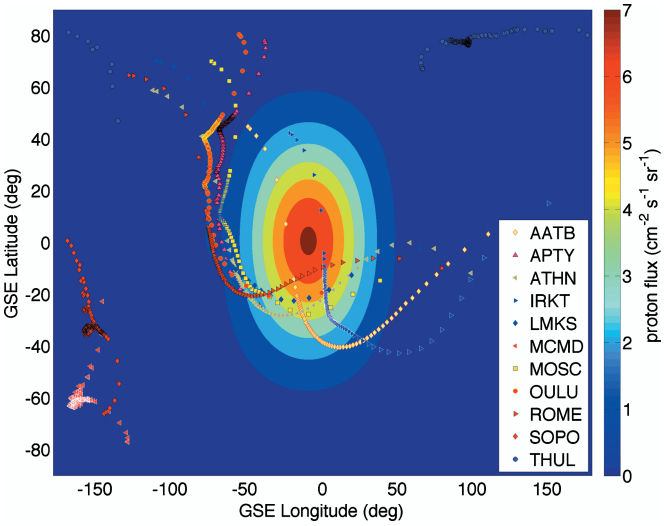

Figure 7. Contour plots of equal integral proton fluxes at the top of the Earth's atmosphere, for proton energies >100 MeV for the time interval 02:00–02:05 UT. The asymptotic directions of viewing for some NMs are also presented (AATB: Alma Ata; APTY: Apatity; ATHN: Athens; IRKT: Irkutsk; LMKS: Lomnicky Stit; MCMD: McMurdo; MOSC: Moscow; OULU: Oulu; ROME: Rome; SOPO: South Pole; THUL: Thule). The integral primary proton flux is given in part cm^{-2} s^{-1} sr^{-1}.

(A color version of this figure is available in the online journal.)

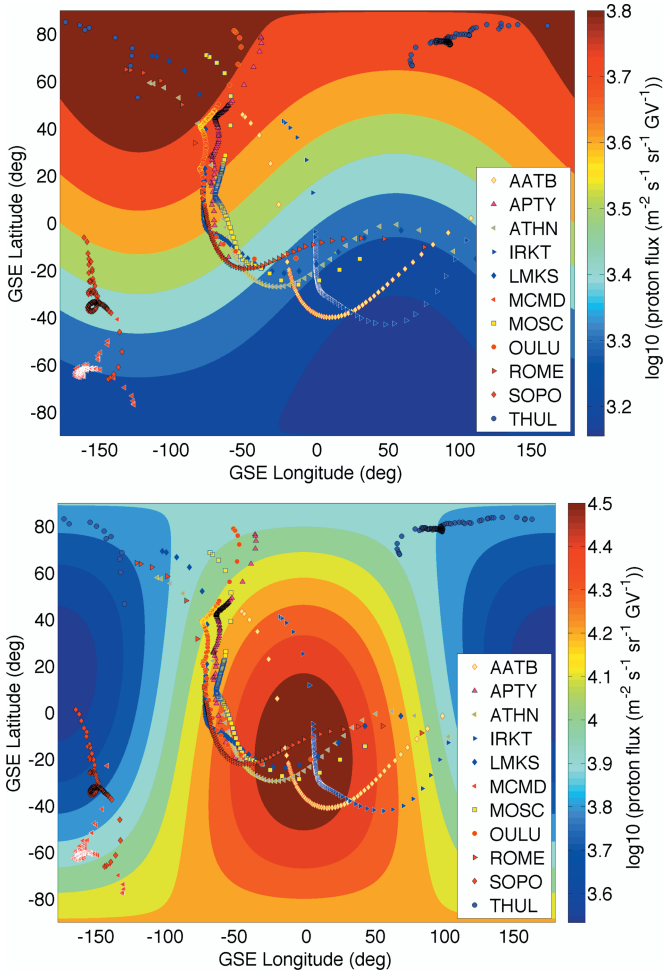

Figure 8. Contour plots of equal differential proton fluxes at the top of the Earth's atmosphere for two different time intervals of the event: 1:50–1:55 UT (upper panel) and 2:15–2:20 UT (lower panel). The asymptotic directions of viewing for some NMs are also presented (AATB: Alma Ata; APTY: Apatity; ATHN: Athens; IRKT: Irkutsk; LMKS: Lomnicky Stit; MCMD: McMurdo; MOSC: Moscow; OULU: Oulu; ROME: Rome; SOPO: South Pole; THUL: Thule). The differential primary proton flux is given in part. m^{-2} s^{-1} sr^{-1} GV^{-1} (note that the scale is logarithmic). Both panels refer to differential proton fluxes corresponding to particles with rigidity equal to 1 GV. Latitude and longitude are given in GSE coordinates (0° corresponds to local noon, and 180° corresponds to local midnight; from the northern hemisphere the rotation is anticlockwise).

(A color version of this figure is available in the online journal.)

(initial phase; Figure 8, upper panel) and 2:15–2:20 UT (near the maximum, Figure 8, lower panel). In the same plot, we also present the asymptotic directions of viewing for some NMs, calculated by the application of the method described in Plainaki et al. (2009b). Both panels in Figure 8 refer to differential primary proton fluxes corresponding to protons with rigidity equal to 1 GV.

In the initial phase of the event, the northern NMs (e.g., OULU, APTY) are found in a more favorable position than the NMs of the southern hemisphere (e.g., Thule: THUL; SOPO; McMurdo: MCMD) with respect to the arrival directions of the energetic solar protons. Indeed, in the time interval 01:50–01:55 UT (Figure 8, upper panel), the asymptotic directions of viewing of the polar NM SOPO are located far enough from the regions of increased primary proton flux concentrated mostly between 40°N and 90°N, for GSE longitudes <–50°E; specifically, the SOPO asymptotic directions of viewing are located farther from that region by more than 40° in latitude. On the contrary, the asymptotic viewing cones of the northern polar NMs, Oulu and Apatity, intersect the regions of the increased primary proton fluxes, and, as a result, these NMs are rendered more favorable for registering the GLE. This spatial configuration has a direct impact in the form of the observed NM intensity time profiles and explains why OULU registered the GLE71 onset before SOPO. Indeed, in Figure 1, left panel, it is seen that at 01:50–01:55 UT, SOPO had not yet started to register the event; at the same time, however, OULU and APTY had already begun to record the GLE, registering increases of ∼2%. The application of our model shows that at 01:50–1:55 UT, the maximum primary solar proton flux was centered above the location 59N, −113E (in GSE coordinates; see Figure 8, upper panel). The beam of the arriving solar protons was not extremely narrow at that time ($n_a = 1.3$), although its direction resulted in a flux spatial distribution with maximum intensities inside the asymptotic cones of the northern NM stations. The observed small difference in absolute values between the ground-level intensity time profiles of the three polar NMs, SOPO, OULU, and APTY (Figure 1, left), at 01:50–01:55 UT, manifests the equivalently small spatial variation of the primary solar proton intensity distribution at that time. We note that, although the spatial variation in the primary solar proton flux is also small (of the order of ∼1.3 part. m^{-2} s^{-1} sr^{-1} GV^{-1}, for $R = 1$ GV), it is big enough to produce observable spatial variations in the secondary SCRs registered at ground level. It is worthwhile to mention that during the same time interval, the mid- and low-latitude NMs of Moscow and Athens/Rome, respectively, had asymptotic directions of viewing that were intersecting the regions of the increased primary solar proton fluxes. However, these stations did not observe a GLE onset at 01:50–1:55 UT, possibly due to extremely low (or absent) primary proton fluxes of rigidities higher than the cut-off rigidities of these stations. Since among these three NMs, MOSC is the one with the lower cut-off rigidity (equal to ∼2.4 GV), we can roughly deduce that the rigidities of the solar protons reaching the Earth on 2012 May 17, could not have been bigger than ∼2.4 GV in the

beginning of the event. This result, obtained through the application of our model using ground-level NM data of the worldwide network, is almost consistent with the estimation by Li et al. (2013), who set an upper rigidity for the solar protons equal to 1.8 GV. We note that Li et al. (2013) used a completely different method that was based on the empirical model by Firoz et al. (2012), assuming a scatter-free proton propagation and using the onsets of the respective flare and CME derived by the observations. Moreover, the GLE71 observations of the NMDB showed that no signal was observed at the NMs with cut-off rigidity >3 GV. The good agreement between all of these estimations is a first-order validation of our model.

After 01:55 UT, the spatial distribution of the primary solar proton flux changes and the solar proton source at the top of the atmosphere moves south (see Figure 8, lower panel). Due to the change in position of the solar proton source, the asymptotic directions of viewing of SOPO at that time are located inside the main contours of the increased primary proton fluxes; therefore, an increase in the count rates of SOPO is registered after 01:55 UT (see Figure 1, left panel). In the following five minute time intervals, due to the moving of the solar proton source, the OULU asymptotic directions of viewing point farther from the regions of the maximum primary fluxes; therefore, OULU becomes less favorable for registering maximum ground level increases. However, since the primary proton fluxes increase dramatically with time (i.e., at 02:15–02:20 UT, the primary solar proton flux, along all latitudes and longitudes, ranges between 4×10^3 and 3×10^4 part. $m^{-2}\,s^{-1}\,sr^{-1}\,GV^{-1}$, for $R = 1$ GV), the OULU asymptotic viewing cones are located inside regions of increased proton fluxes. Consequently, the GLE is indeed being registered by both northern and southern NMs.

Consistent with the results of our model, in the time interval 02:00–2:15 UT, the SOPO NM registers relatively higher ground-level count rates than the OULU and APTY NMs, due its favorable asymptotic directions of viewing with respect to the main solar proton arrival direction. At the time interval 02:15–02:20 UT, the difference in the intensities registered at SOPO and OULU are smoothed (see Figure 1, left); moreover, APTY registers higher count rates than SOPO. This behavior, obtained from the ground-level NM time profiles, can be explained using the outputs of our model, in terms of the arrival direction of the primary flux at the top of the atmosphere and the asymptotic directions of viewing of each NM at this specific time interval. Figure 8 (lower panel) shows that, in the time interval 02:15–02:20 UT, the position of the primary solar proton source outside the atmosphere mostly favors the northern NMs for ground-level registration of the event. Therefore, APTY and OULU are, in general, more favored for registering the GLE. However, we note that in this specific time interval, only APTY registers slightly larger count rates than SOPO; OULU registers count rates that are slightly smaller (∼1%) than SOPO (see Figure 1, left panel). Since the locations of both APTY and OULU do not differ significantly (resulting in similar asymptotic directions of viewing, as seen in Figure 8), we believe that this fact is due to the low altitude at which the OULU NM is located (∼15 m) with respect to the relatively higher altitude of the APTY NM (∼177 m). This factor, together with the fact that the primary flux at the top of the atmosphere was small during GLE71 (in comparison with other past GLEs, e.g., GLE69, GLE60), renders the ground-level registration extremely sensitive to the altitude at which the NM is located. In the time interval 02:15–02:20 UT, the angular distribution of the primary solar proton flux is wide ($n_a = 1.6$); contrary to the initial phase of the event, when a wide angular flux distribution was also present, the primary solar proton intensities at this time interval are significantly increased in absolute values (i.e., up to 3×10^4 part. $m^{-2}\,s^{-1}\,sr^{-1}\,GV^{-1}$), meaning an increase by almost four orders of magnitude with respect to the flux registered during the initial phase of the GLE. Therefore, although the northern NMs seem to be more favorable for GLE registration, the NMs of the southern hemispheres do register high count rates. In the following time intervals, primary and secondary SCR fluxes significantly decrease.

5. CONCLUSIONS

In this paper, we modeled the first GLE of the 24th solar activity cycle by applying the NMBANGLE PPOLA model to the data of 29 NMs. Our main results are summarized in the following points.

1. The primary SCR spectrum at the top of the Earth's atmosphere was rather soft, with a spectral index (in rigidity) ranging between −2.1 and −3.8, consistent with the estimations based on satellite observations (e.g., Li et al. 2013).
2. The primary SCR spectrum calculated by our model supports the CME shock driven particle, although a direct flare contribution cannot be excluded.
3. The NM time intensity profiles during GLE71 are interpreted on the basis of the primary SCR flux spatial distribution at the top of the Earth's atmosphere; in the initial phases of the event, the northern NMs were more favorably positioned with respect to the GLE source, and hence, they registered the event prior to the southern NMs.
4. The integral SCR fluxes calculated by our model are in good agreement with the *GOES* observations, and hence, a realistic estimation of the >100 MeV flux value is also provided.

Although our model explains various observational facts of GLE71, we underline some important details of our method that determine the interpretation of the results. In our model, all of the differences among the ground-level intensities registered by the various NMs are attributed to the related position of their asymptotic directions of viewing with respect to the position of the solar proton beam outside the atmosphere and to the cut-off rigidity of each NM. The position of the GLE source outside the atmosphere has often been considered to be the most significant factor determining the propagation and final registration of the secondaries at ground level; indeed, up to now, this assumption has been considered in numerous modeling efforts of different GLEs (see Vashenyuk et al. 2011; Plainaki et al. 2007, 2010; Bombardieri et al. 2007; Balabin et al. 2013). However, other phenomena, like the diffusion of the secondary particles inside the atmosphere, could also have a role in the interpretation of the ground-level intensity time profiles during a GLE. Indeed, inside our model, we simulate the atmosphere effect through the use of the Dorman coupling functions, also used in the past by other models, depending on the location and altitude of each NM as well as the solar activity (Plainaki et al. 2010). However, it should be noted that the functions used inside the NMBANGLE PPOLA model were firstly created using data from the sea level NMs, and afterward, they were parameterized. Moreover, inside these functions, no location-dependent atmospheric density is included; such an input could change the properties of the solar proton propagation inside the atmosphere, the mean free path, and the properties of the

cascade, resulting in variations of the ground-level intensity time profiles. During large (in solar proton energy) GLEs, this factor could be rendered less significant, but during low energy GLEs (i.e., higher collision cross section), the specific properties of the atmosphere above an NM could influence the registered ground-level count rates.

The derivation of the GLE71 properties through the NMBANGLE PPOLA application is an example of how NM network data can be efficiently used for space weather modeling and specifically for getting information that cannot be directly obtained by space instruments (e.g., the higher energy part of the SCR spectrum during the event). In the context of a neutron monitor network of widely distributed stations, the NMBANGLE PPOLA represents a new useful tool for the study of solar physics and space weather, providing complementary information on SCRs to that obtained by space techniques.

The authors acknowledge all colleagues at the NM stations who kindly provided us with the data used in this study: Alma Ata, Apatity, Athens, Baksan, Emilio Sergè Observatory, Fort Smith, Inuvik, Irkutsk, Irkutsk 2, Irkutsk 3, Jungfraujoch, Jungfraujoch-1, Kerguelen, Kiel, Lomnický Štít, Magadan, McMurdo, Moscow, Nain, Norilsk, Newark, Oulu, Peawanuck, Rome, South Pole, Terre Adeliè, Thule, Tixie Bay, and Yakutsk. We acknowledge the High-resolution Neutron Monitor NMDB database, founded under the European Union's FP7 Program (contract No. 213007) for providing cosmic ray data. We are grateful to the IZMIRAN cosmic ray group, and particularly to Drs. Anatoly Belov, Eugenia Eroshenko, and Victor Yanke for providing us the code for the calculation of the neutron monitor asymptotic directions of viewing. The authors also thank Dr. Stefano Massetti for useful advice on technical issues regarding the calculation of the particle trajectories inside the Earth's magnetic field and Dr. Tsyganenko for providing the GEOPACK routines. This work was partially supported by the ASI/INAF contract no. I/022/10/0.

REFERENCES

Abbasi, R., Abdou, Y., Ackermann, M., et al. 2013, NIMPA, 700, 188
Adriani, O., Barbarino, G. C., Bazilevskaya, G. A., et al. 2011, ApJ, 742, 102
Balabin, Y. V., et al. 2013, in Proc. 33rd Inter. Cosmic Ray Conf. (http://www.cbpf.br/∼icrc2013/papers/icrc2013-0021.pdf)
Bazilevskaya, G. A., Flueckiger, E., Makhmutov, V. S., et al. 1996, Radiat. Meas., 26, 443
Bazilevskaya, G. A., Mayorov, A. G., & Mikhailov, V. V. 2013, in Proc. 33rd Inter. Cosmic Ray Conf. (http://www.cbpf.br/∼icrc2013/papers/icrc2013-0332.pdf)
Belov, A. V., Eroshenko, E., Mavromichalaki, H., Plainaki, C., & Yanke, V. 2005a, AnGeo, 23, 2281
Belov, A. V., Eroshenko, E. A., Mavromichalaki, H., Plainaki, C., & Yanke, V. G. 2005b, in Proc. 29th Inter. Cosmic Ray Conf., Vol. 1, ed. S. Acharya, S. Gupta, P. Jagadeesan et al. (Mumbai: Tata Institute of Fundamental Research), 189
Berezhko, E. G., & Taneev, S. N. 2003, Russ. Astron. Lett., 29, 601
Bieber, J. W., Dröge, W., Evenson, P. A., et al. 2002, ApJ, 567, 622
Bombardieri, D. J., Michael, K. J., Duldig, M. L., & Humble, J. E. 2007, ApJ, 665, 813
Bütikofer, R., & Flückiger, E. O. 2013, JPhCS, 409, 012166
Bütikofer, R., Flückiger, E. O., Desorgher, L., Moser, M. R., & Pirard, B. 2009, AdSpR, 43, 499
Cane, H. V., Richardson, I. G., & von Rosenvinge, T. T. 2010, JGR, 115, A08101
Carbone, et al. 2013, in Proc. 33rd Inter. Cosmic Ray Conf. (http://www.cbpf.br/∼icrc2013/papers/icrc2013-0845.pdf)
Cramp, J. L., Duldig, M. L., & Humble, J. E. 1995, in Proc. 24th Inter. Cosmic Ray Conf., ed. N. Iucci & E. Lamanna (Rome: International Union of Pure and Applied Physics), 248
Cramp, J. L., Duldig, M. L., & Humble, J. E. 1997, JGR, 102, 4919
Damiani, A., Diego, P., Laurenza, M., Storini, M., & Rafanelli, C. 2009, AdSpR, 43, 28
Dorman, L. I. 2004, Astrophysics and Space Science Library, Vol. 303 (Dordrecht: Kluwer)
Dorman, L. I., Danilova, O. A., Iucci, N., et al. 2008, AdSpR, 42, 510
Ellison, D. C., & Ramaty, R. 1985, ApJ, 298, 400
Firoz, K. A., Gan, W. Q., Moon, Y.-J., & LI, C. 2012, ApJ, 758, 119
Gopalswamy, N., Yashiro, S., Kaiser, M. L., et al. 2001, JGR, 106, 207
Gopalswamy, N., Xie, H., Akiyama, S., et al. 2013, ApJL, 765, L30
Grigoryev, V. G., Starodubtsev, S. A., & Evstafieva, M. A. 2013, JPhCS, 409, 012173
Humble, J. E., Duldig, M. L., Smart, D. F., & Shea, M. A. 1991, GeoRL, 18, 737
Kudela, K. 2013, JPhCS, 409, 012017
Lee, M. A., Mewaldt, R. A., & Giacalone, J. 2013, SSRv, 173, 247
Li, C., Firoz, K. A., Sun, L. P., & Miroshnichenko, L. I. 2013, ApJ, 770, 34
Liu, C., Lee, J., Karlický, M., et al. 2009, ApJ, 703, 757
Lopate, C. 2006, in Solar Eruptions and Energetic Particles, ed. N. Gopalswamy, R. Mewaldt, & J. Torsti (Geophysical Monograph Series, Vol. 165; Washington, DC: AGU), 283
McCracken, K. G., Moraal, H., & Shea, M. A. 2012, ApJ, 761, 101
Mewaldt, R. A., Looper, M. D., Cohen, C. M. S., et al. 2012, SSRv, 171, 97
Miroshnichenko, L. I. 2003, Radiation Hazard in Space (Astrophysics and Space Science Library, Vol. 297 (Dordrecht: Kluwer)
Miroshnichenko, L. I., & Pérez-Peraza, J. A. 2008, IJMPA, 23, 1
Miroshnichenko, L. I., Vashenyuk, E. V., & PérezPeraza, J. A. 2013, Ge&Ae, 53, 541
Muraki, Y., Matsubara, Y., Masuda, S., et al. 2008, APh, 29, 229
Oreshina, A. V., & Somov, B. V. 2011, AsTL, 37, 726
Pérez-Peraza, J. 2011, in Proc. 32nd Inter. Cosmic Ray Conf., SH1-SH2: Solar and Heliospheric Phenomena, Vol. 10 (Beijing: Inst. of High Energy Physics), 149
Picozza, P., Galper, A. M., Castellini, G., et al. 2007, APh, 27, 296
Plainaki, C., Belov, A., Eroshenko, E., Mavromichalaki, H., & Yanke, V. 2007, JGRA, 112, 4102
Plainaki, C., Mavromichalaki, H., Belov, A., Eroshenko, E., & Yanke, V. 2009a, AdSpR, 43, 474
Plainaki, C., Mavromichalaki, H., Belov, A., Eroshenko, E., & Yanke, V. 2009b, AdSpR, 43, 518
Plainaki, C., Mavromichalaki, H., Belov, A., et al. 2010, SoPh, 264, 239
Reames, D. V. 1999, SSRv, 90, 413
Shea, M. A., & Smart, D. F. 1982, SSRv, 32, 251
Shen, C., Li, G., Kong, X., et al. 2013, ApJ, 763, 114
Signoretti, F., & Storini, M. 2013, INAF Report IAPS-2013–05 (Rome, Italy: Institute for Space Astrophysics and Planetology)
The IceCube Collaboration 2013, arXiv:1309.7006v2
Tsyganenko, N. A. 1989, P&SS, 37, 5
Vashenyuk, E. V., Balabin, Y. V., & Gvozdevsky, B. B. 2011, ASTRA, 7, 459